RSC Advances

ROYAL SOCIETY OF CHEMISTRY

www.rsc.org/advances

Mediator-free Total Cholesterol Estimation using Bi-enzyme Functionalized Nanostructured Gold Electrode

Rachna Sharma,[a,b] R. K. Sinha,[b] Ved Varun Agrawal[a,*]

[a]Biomedical Instrumentation Section, National Physical Laboratory, New Delhi 110012, India

[b]Department of Applied Physics, Delhi Technological University, New Delhi 110042, India

Abstract

We report the fabrication of bienzyme functionalized nanostructured Au electrode for the mediator-free determination of total cholesterol. The one-step electrochemical route for the synthesis, functionalization and deposition of Au nanostructures via electroreduction of gold chloride onto the indium tin oxide (ITO) coated glass plates has been proposed. The covalent biofunctionalization of the optimized Au electrode has been done with cholesterol esterase (ChEt) and cholesterol oxidase (ChOx) to investigate the kinetic parameters and the sensing characteristics. The ChEt-ChOx/Glu-NanoAu/ITO bioelectrode shows surface-controlled electrode reaction with electron transfer coefficient and charge transfer rate constant of 0.68 and 7.09 s^{-1}, respectively. Under the optimal conditions, the bioelectrode undergoes direct electron transfer reaction and exhibits high sensitivity of 0.53 A M^{-1} cm^{-2} and low detection limit of 1.57 μM for cholesterol ester without use of any redox mediator. In addition, the kinetic analysis reveals that the bioelectrode exhibits surface concentration as 8.82 $\times 10^{-12}$ mol cm^{-2}. The sensor has also been validated with clinical samples. The proposed biosensor shows good sensitivity, stability and selectivity towards total cholesterol and may thus find implications towards the fabrication of a biosensing device.

Keywords: gold chloride, electrochemical synthesis, kinetic analysis, total cholesterol biosensor, mediator-free

*E-mail: ved.varun@gmail.com, Tel: +91-11-45609489

1. Introduction

The unique electronic, optical and catalytic properties of gold nanoparticles (NPs) have indulged researchers in developing simpler methods for synthesis of various nanostructures and intensive study of their applications.[1] The tunable surface chemistry, morphology, optical, catalytic and electrocatalytic properties of gold nanostructures make them ideal for a variety of sophisticated technology applications such as organic photovoltaics,[2] optical sensing,[3] drug delivery[4] and other biomedical applications.[5, 6] Duncan et al. have reported the tunability of the Au NPs monolayer allowing complete control of surface properties for targeting and release of drugs using these nanocarriers.[7] The remarkable electrocatalytic activity, surface plasmon resonance and biocompatibility of nano-gold make it promising for applications in biochemical sensing and medical diagnostics.[8] Si et al have reported the fabrication of a highly sensitive glucose biosensor based on covalently assembled high density Au nanostructures.[9] Although bulk gold is a poor catalyst, nanometer-sized gold exhibits excellent electrocatalytic activity and the electrochemical properties can be tuned by the control of size and shape as per desired application. One important attribute of the nanosized catalysts is the high surface area and interface-dominated properties that differ from atomic, molecule and bulk counterparts.[10] The Au nanostructures provide direct electrical communication between the biomolecules and the electrode resulting in direct electron transfer across the interface. Shi et al have reported the fabrication of aloe-like gold micro/nanostructures for ultrasensitive DNA recognition.[11] Liu et al. have reported the direct electron transfer of copper, zinc-superoxide dismutase (Cu, Zn-SOD) onto nanospherical, nanorodlike, and nanopyramidal gold nanostructures resulting in the mediator-free superoxide anion biosensor.[12]

The integration of gold nanostructures into thin films is particularly important for multivalent applications in electrochemistry and bioelectronics for the development of biomedical and opto-electronic nanodevices. A precise control over arrangement of NPs onto the substrate is of utmost importance. Several methods for preparation of nanostructured Au films have been reported, however, most of them involve multiple steps of synthesis, surface modification and assembly of NPs. However, electrochemical technique offers rapid and uniform deposition of desired materials and their composites by optimization of parameters such as solution concentration, applied potential, pH etc.[13] The electrodeposition of nanomaterials involves the use of hard templates such as anodic aluminium oxide and highly ordered pyrolytic

graphite etc. Soft templates such as polymers or surfactants can also be used as shape controllers to direct the preferential growth of Au nanoparticles into the desired shapes. Huang et al. have reported the electrochemical tuning of the size of Au nanoparticles using the tetradodecylammonium bromide surfactant.[14] The template-free electrodeposition of Au nanostructures can be achieved using Au precursors like $HAuCl_4$ and $Au(PPh_3)Cl$. Wang et al. have reported the fabrication of flower-like nanoparticles with nanoplates as the building blocks using $HAuCl_4$ at pH 5.0.[15] Sharma et al have reported the deposition of different Au nanostructures using $Au(PPh_3)Cl$ by variation of the concentration of capping ligand.[16]

The efficient immobilization of biomolecules onto the nanostructured surface is crucial for the fabrication of biosensors. The desired functionalization of the NPs can be accomplished during synthesis by addition of a suitable capping ligand with terminations like NH_2, COOH etc, which can be utilized for the covalent attachment of biomolecules. The biofunctionalized Au nanostructures enable wide range of biomedical applications. For instance, Luo et al have demonstrated the multiple applications of protein and peptide-protected Au nanocrystals (size ~2 nm) as optical probes for bioimaging and biosensing and constructing antimicrobial and therapeutic agents.[17] The utilization of cysteamine functionalized nanostructured Au electrode for the immobilization of enzyme molecules may improve the efficacy of biosensors due to high loading of the covalently linked enzymes and facilitation of direct electron transfer from redox centres of biomolecules to the electrode.[16]

In this manuscript, we report the deposition of Au nanostructures onto the ITO electrodes using chronoamperometric technique. The electrocatalytic activity of the nanostructured Au electrode has been optimized through the variation of cysteamine concentration during synthesis and the kinetic parameters of Au electrodes have been evaluated using cyclic voltammetry. The optimized Au electrode has been utilized for the covalent immobilization of dual enzymes (ChEt and ChOx) in order to investigate the interfacial kinetics and the sensing performance of the bienzymatic electrode towards total cholesterol.

2. Materials and Methods

Cholesterol esterase, cholesterol oxidase, cholesterol oleate, tetrachloroauric acid ($HAuCl_4$), trichloroacetic acid, triton X-100 and cysteamine hydrochloride were purchased from Sigma-Aldrich. All reagents were of analytical grade and used without further purification. De-ionized water (Milli Q 10 TS) with resistivity >18.2 MΩ-cm was used for preparing all aqueous

solutions. Indium-tin-oxide (ITO) coated glass plates were purchased from Balzers, UK, (Baltracom 247 ITO, 1.1 mm thick) with a sheet resistance and transmittance of 25 Ω sq^{-1} and 90%, respectively. The stock solution of cholesterol oleate was prepared in 10% triton X-100 and stored at 4°C.

2.1 Instrumentation

Morphological studies have been carried out using Atomic Force Microscope (Nanoscope, Bruker) and Scanning Electron Microscope (SEM, FEI Nova 600 microscope). Fourier Transform Infrared (FT-IR) studies have been carried out on Perkin Elmer, Spectrum BX II spectrophotometer. Contact angle measurements have been carried out using OCA 15 EC (DataPhysics). The electrochemical experiments have been conducted on Autolab PGSTAT 302N System (Ecochemie, The Netherlands) in three electrodes system with platinum as auxiliary, Ag/AgCl as reference and ITO substrate as working electrode.

2.2 Fabrication of Nanostructured Au Electrode

The ITO substrates have been modified with different Au nanostructures using chronoamperometric technique. The aqueous solution of $HAuCl_4$ (0.10 mM) and trichloroacetic acid (50 mM) has been used as an electrolyte. For the fabrication of nanostructured Au films, deposition potential and deposition time have been optimized as -1 V and 300 s, respectively. The morphology of Au electrodes has been controlled with variation of cysteamine concentrations in the electrolyte (i.e. 0.025 mM, 0.125 mM and 0.625 mM) [Scheme 1].

2.3 Fabrication of the Bioelectrode

The optimized Au electrode has been utilized for the fabrication of bienzymatic electrode for detection of cholesterol oleate. The amine-functionalized nanostructured Au electrode was dipped in 0.5% glutaraldehyde solution for 4 h, followed by rinsing with distilled water. The modified Au film was then incubated with 100 µL of phosphate buffer solution (PBS; pH 7.4) containing ChEt and ChOx (1 mg/mL) for overnight at 4°C. The aldehyde group at the surface binds covalently with the amine group of the enzyme molecules resulting in the fabrication of ChEt-ChOx/Glu-NanoAu/ITO bioelectrode. The loosely bound enzyme molecules were washed off with PBS buffer and the bioelectrode was stored at 4°C.

3. Results and Discussion

3.1 AFM Studies

Fig. 1 shows the structural features of electrochemically deposited Au nanostructures on ITO coated glass plates. The reduced $HAuCl_4$ molecules assemble into plate-like structures (average length ~800 nm, aspect ratio ~ 2.5) stacked onto each other in the absence of capping agents [Fig. 1(a)]. On application of electric potential, the Au^{3+} ions present in the electrolyte drift towards the ITO substrate where Au^{3+} reduces to Au^0, resulting in the nucleation of Au NPs. The structure of reduced Au is determined by the current across the electrode-electrolyte interface. In the absence of any capping ligand, the assembly of the reduced Au into elongated structures owes to the slow rate of electrochemical reaction. On incorporation of the capping ligand (cysteamine) into the electrolyte, the agglomeration reduces due to increase in the electrochemical current. In presence of 0.025 mM cysteamine, the formation of necks in the elongated rod-like structures of Au (average length ~800 nm, aspect ratio ~2.5) have been observed due to the diffusion of cysteamine molecules [Fig. 1(b)][18]. Spherical Au NPs act as building blocks for these structures and no stacking is observed. The rods fragment into circular structures of ~400 nm with the cysteamine concentration of 0.125 mM [Fig. 1(c)]. With further increase of cysteamine concentration, the coverage of cysteamine molecules onto Au NPs restricts their assembly into secondary structures and densely packed spherical Au NPs are obtained [Fig. 1(d)]. The Au NPs assemble into various structures depending on the concentration of cysteamine molecules to attain minimum surface energy. With sufficient cysteamine molecules, the film of densely packed Au NPs is obtained.

3.2 Wettability Studies of Nanostructured Au films

Contact angle measurements have been carried out to test the surface wettability of the nanocrystalline Au films [Fig. 2A]. Water has been used as the dispersant and sessile drop method has been used to evaluate the contact angle of water drop with the Au surface. It has been observed that the Au film prepared in absence of cysteamine is highly hydrophobic with contact angle of 135° [Fig. 2A(a)]. It do not allow water drop to spread onto its surface. However, the adsorption of aqueous thiol (cysteamine) onto Au NPs results in decrease in the contact angle of the nanocrystalline films. When there is deficit of cysteamine, the hydrophobic nature of the film prevails due to incomplete coverage of the NPs with cysteamine which results in contact angle of 97° [Fig. 2A(b)]. As the amount of cysteamine increases, more surfaces of the NPs get covered with the aqueous thiol making the film more hydrophilic with contact angle of water being 57° [Fig. 2A(c)]. With excess of cysteamine, all the facets of NPs are well covered

which allows smooth spreading of water droplet on the surface of film and the contact angle reduces to 46° [Fig. 2A(d)]. This shows that cysteamine imparts hydrophilicity to the nanostructured Au films, which is essential for the immobilization of biomolecules. The contact angle of water drop with Au surface decays exponentially with the amount of cysteamine and the evolution of hydrophilic character of Au films is due to the increase of amine terminations at the Au surface[19].

3.3 FTIR Studies

Figure 2B shows the FTIR spectra of NanoAu/ITO electrode, Glu-NanoAu/ITO electrode and ChEt-ChOx/Glu-NanoAu/ITO bioelectrode. The peaks at 684 cm^{-1}, 892 cm^{-1} and 996 cm^{-1} correspond to C-S stretch, NH_2 stretch and C-N in primary aliphatic amines, respectively, confirming the presence of cysteamine molecules in the Au film [Fig. 2B(i)]. The peaks at 449 cm^{-1}, 566 cm^{-1}, 1401 cm^{-1} and 1518 cm^{-1} arise from the alkyl group (C_nH_{2n+1}), C-Cl stretch, C-H stretch and $–COO^-$ antisymmetric stretch from the trichloroacetic acid molecules[20]. In figure 2B(ii), the peaks at 1094 cm^{-1}, 1431 cm^{-1}, 1507 cm^{-1}, 1692 cm^{-1}, 1814 cm^{-1} corresponding to C-NH_2 stretch, C-N stretch, NH^{3+} deformation, NH_2 stretch and C=O stretch, respectively, confirm the formation of covalent amide bond between the amine-terminated Au surface and the glutaraldehyde. The peaks at 2872 cm^{-1} and 2933 cm^{-1} correspond to C-H antisymmetric and symmetric stretch. Further in figure 2B(iii), the peaks at 826 cm^{-1}, 1048 cm^{-1} and 2335 cm^{-1} corresponding to P-O stretch, P-OH stretch and P-H stretch, respectively, arise from the enzyme molecules[20].The peaks at 1921 cm^{-1} and 2106 cm^{-1} arise from the combination of NH^{3+} torsion and NH^{3+} antisymmetric deformation and the peaks at 1592 cm^{-1} and 1723 cm^{-1} arise from the NH_2 stretch and C=O stretch, respectively, due to the amide bond formation between glutaraldehyde and the enzyme molecules[20]. This confirms the covalent attachment of ChEt-ChOx molecules to the nanostructured Au surface.

3.4 Morphological Characterization of the Bioelectrode

Morphological studies have been carried out to investigate the loading of enzyme molecules onto the nanostructured Au electrode and the SEM images are displayed in Figure 3. The micrograph [Fig. 3(a)] reveals the dense packing of the uniform-sized Au NPs onto the ITO surface in agreement with the AFM image. The morphology of the nanostructured Au electrode changes to spherical globules on incubation with glutaraldehyde [Fig. 3(b)]. Further, the morphology change from globular spheres of glutaraldehyde to densely packed agglomerates on incubation with the

enzyme solution [Fig. 3(c)]. This confirms the adsorption of enzyme molecules onto the nanostructured Au electrode, leading to the formation of the bioelectrode.

3.5 Electrochemical Characterization of Nanostructured Au Films

Figure 4(A) shows the current response as a function of time during electrochemical deposition of Au nanostructures. The current across the electrode-electrolyte system is ~10 mA in the absence of cysteamine and the elongated plate-like structures result. On incorporation of cysteamine, the current has been found to increase. This results in higher drift of the $HAuCl_4$ molecules towards the electrode and thus faster electroreduction of Au^{3+} ions. The subsequent addition of cysteamine in the electrolytic solution leads to increase in current to ~20 mA. The amount of cysteamine molecules and the rate of electroreduction of Au^{3+} ions govern the assembly of reduced Au on the ITO surface. The Au NPs assemble into different nanostructures in order to attain minimum surface energy. The higher amount of cysteamine results in the deposition of smaller nanostructures.

The cyclic voltammetric studies have been carried out to examine the electrochemical behaviour of the nanostructured Au films in PBS without any redox mediator [Fig. 4(B)]. The nanostructured Au films exhibit redox peaks at ~0.2 V and ~0.0 V, which are attributed to the oxidation and subsequent reduction of gold oxide (AuO_x) as a result of electronic polarization[21]. However, the difference in magnitudes of anodic and cathodic current indicates the chemical irreversibility of the surface reaction. With the incorporation of cysteamine, the sulphur ions at the surface of Au nanostructures further facilitate the electrochemical oxidation-reduction of Au, resulting in enhanced electrochemical current[22]. Also, the higher surface area provided by smaller Au nanostructures results in faster electron transfer kinetics leading to increase in redox current.

3.6 Kinetic Studies of Au electrode and Bioelectrode

The cyclic voltammetric studies for the NanoAu/ITO electrode and ChEt-ChOx/Glu-NanoAu/ ITO bioelectrode as a function of scan rate (10-100 mVs^{-1}) have been carried out to investigate the interfacial phenomena [Fig. 4C, 4D]. The shift of the anodic potential towards the positive value with the increase of scan rate implies that the electrochemical reaction is either quasi-reversible or irreversible in nature. As the anodic and cathodic current vary linearly with square root of the scan rate (above 30 mVs^{-1}), this suggests that the electrochemical reaction is quasi-reversible at low scan rates (<30 mVs^{-1}) and irreversible above 30 mVs^{-1}.

Further, the anodic peak potential varies linearly as a logarithmic function of scan rate in the range from 10-100 mVs^{-1}[Fig. 4C, 4D (inset (i))]. Though, the shift in the cathodic potential isn't appreciable but on magnifying the curves, slight shift can be seen. Using Laviron's equations, the value of electron transfer coefficient (α), for n number of electrons, has been determined from the anodic and cathodic slopes of $2.303RT/(1-\alpha)nF$ and $-2.303RT/\alpha nF$, respectively[23]. The value of α increase from 0.50 to 0.65 for the Au electrodes fabricated with the subsequent increase of cysteamine concentration [Table 1]. The charge transfer rate constant (k_s) has been calculated using Eq. (1):

$$\ln k_s = \alpha \ln(1-\alpha) + (1-\alpha)\ln\alpha - \ln\left(\frac{RT}{nF\nu}\right) - \alpha(1-\alpha)\left(\frac{nF\Delta E_p}{RT}\right) \quad \ldots(1)$$

The value of k_s decreases from 68.39 to 3.55 s^{-1} for the Au electrodes fabricated with subsequent increase of cysteamine concentration [Table 1]. This is due to slight increase in the peak separation for the Au electrodes with the increase of cysteamine concentration.

For a surface-controlled process, the surface concentration of ionic species (Γ) can be estimated using Brown-Anson model [Eq. (2)]:[24]

$$I_p = n^2F^2\nu A\Gamma(4RT)^{-1} \quad \ldots(2)$$

where I_p/ν can be obtained from the linear regression of anodic peak potential versus scan rate curve. The surface concentration of ionic species for Au electrodes with increasing cysteamine concentration increases from 1.30×10^{-13} to 8.22×10^{-12} mol cm^{-2}. This is in accordance with the higher loading of gold nanostructures onto the ITO substrate with the increase of cysteamine concentration. The nanostructured Au electrode (0.625 mM cysteamine) with higher surface concentration of electroactive species has been used for fabrication of the enzymatic bioelectrode.

After ChEt-ChOx immobilization, the value of k_s increases from 3.55 to 7.09 s^{-1}, respectively. This is attributed to the establishment of electrical contact between redox centres of enzyme molecules and the surface of Au nanostructures which facilitates electronic and ionic transport across the interface. Also, the surface concentration of ionic species has been found to increase ten-fold from 8.22×10^{-13} to 8.82×10^{-12} mol cm^{-2} after enzyme immobilization [Table 1]. This reveals the chemisorption of enzyme molecules onto the nanostructured Au electrodes resulting in more number of active sites onto the nanostructured Au matrix. The ChEt-

ChOx/Glu-NanoAu/ITO bioelectrode fabricated using optimized Au electrode (0.625 mM cysteamine) has been utilized for the electrochemical detection of cholesterol oleate.

3.7 Cyclic Voltammetric Response of the Bioelectrode

The fabrication of ChEt-ChOx/Glu-NanoAu/ITO bioelectrode has been investigated at each modification step using cyclic voltammetry in PBS [Fig. 5A]. The ITO electrode has no current response in the potential region from -0.7 V to +0.7 V. The redox peaks from Au nanostructures at ~0.2 V and ~0.0 V disappear on incubation of the Au film with glutaraldehyde and the remarkable decrease in current was observed. The insulating layer of glutaraldehyde onto nanostructured Au electrode results in sluggish electron transportation across the interface. After ChEt-ChOx immobilization, the redox peaks reappear at ~0.3 V and ~0.0 V, which are attributed to the electronic communication of flavin adenine dinucleotide (FAD) cofactor of enzyme molecules with the Au nanostructures[25]. The electrical wiring of FAD molecules and Au nanostructures results in direct electron transfer phenomenon and thus paves the way for fabrication of mediator-free total cholesterol biosensor.

The electrochemical response of the ChEt-ChOx/Glu-NanoAu/ITO bioelectrode towards different concentrations of cholesterol ester (oleate) has been studied [Fig. 5B]. The anodic current has been found to increase with the increasing concentrations of cholesterol ester (10-500 $mgdl^{-1}$). In the proposed biochemical reaction, cholesterol esters are hydrolyzed via cholesterol esterase into cholesterol (or 3β-hydroxysteroids) and fatty acid. ChOx then catalyzes the oxidation of cholesterol (3β-hydroxysteroids) to the intermediate product Δ5-6-ene-3β-ketosteroid (cholest-5-en-3-one). The isomerization of the intermediate product results into Δ3-4-ene-3β-ketosteroid (cholest-4-en-3-one)[26]. The FAD cofactor gets reduced to $FADH_2$ in the process and in order to re-oxidize, the direct exchange of electrons occur with the nanostructured Au electrode resulting in increase in peak current with the increasing concentrations of cholesterol oleate. The anodic peak current of the ChEt-ChOx/Glu-NanoAu/ITO bioelectrode plotted as a logarithmic function of cholesterol concentration reveals the linearity range as 10–500 mg dl^{-1} (within 2% error) with standard deviation and correlation coefficient of 0.28 μA and 0.99, respectively [Fig. 5C]. The sensitivity of the ChEt-ChOx/Glu-NanoAu/ITO bioelectrode exhibited by the slope of the linear regression curve is 0.53 A M^{-1} cm^{-2} and the detection limit calculated using 3*SD/Sensitivity is 1.57 μM. The apparent Michaelis–Menten constant, which is an indication of the enzyme-substrate kinetics, has been evaluated from the Lineweaver-Burk

equation and has been calculated to be as 0.63 mM[27]. The small K_m^{app} value indicates that the immobilized enzymes possess high enzymatic activity and that the fabricated biosensor exhibits a high affinity for cholesterol. Table 2 summarizes the biosensing characteristics of the mediator-free cholesterol biosensors reported in literature. It can be seen that the sensitivity of the proposed total cholesterol biosensor is manifold higher and the limit of detection is appreciably lower as compared to those reported in literature. Also, the proposed biosensor exhibits comparable value of K_m^{app} and an extended linear range for esterified cholesterol detection.

The effect of potential interferents on the total cholesterol measurements has been investigated by taking the solution containing 1 : 1 ratio of cholesterol ester (200 mg dl^{-1}) and interferents such as glucose (5 mM), urea (1 mM), uric acid (0.1 mM) and ascorbic acid (0.05 mM) [Fig. 5D]. In the presence of interferents, 2-3% change of current has been observed from the CV response of the ChEt-ChOx/Glu-NanoAu/ITO bioelectrode which has been calculated using following equation: %inter = I_{chol} - I_{Int}/I_{chol}, where I_{chol} and I_{int} are the changes in current corresponding to the cholesterol ester and the1:1 mixture of cholesterol ester with interferent. This shows that the proposed biosensor is highly selective towards total cholesterol.

3.8 Clinical Sample Analysis

The response studies of the ChEt–ChOx/Glu-NanoAu/ITO bioelectrode were carried out for five clinical samples with varying cholesterol concentrations. Serum samples from patients along with clinical data of cholesterol levels were collected from Dr. Arvind's Family Clinic, New Delhi (India). In comparison to the standard cholesterol concentration, it has been observed that the ChEt–ChOx/Glu-NanoAu/ITO bioelectrode shows a minute difference of 3-5% in current response during cholesterol detection in clinical serum samples [Fig. 6A]. The current versus logarithmic value of concentration shows a nearly linear response with clinical patient samples [Fig. 6B] and the sensitivity (0.48 $AM^{-1}cm^{-2}$) shows ~ 10-11% compared to that for the standard cholesterol concentrations, which is acceptable. This indicates great potential of the bioelectrode towards the development of point of care diagnostics. Thus, these results indicate that this novel biosensor has the potential to detect cholesterol directly in human serum samples.

The shelf life and reproducibility of the ChEt-ChOx/Glu-NanoAu/ITO bioelectrode have been investigated using cyclic voltammetry. The bioelectrode exhibits only 6% reduction in peak current after 8 weeks for 100 mg dl^{-1} cholesterol concentration when stored at 4°C indicating good stability [Fig. 7A]. To check the reproducibility of the proposed biosensor, six

bioelectrodes were prepared under similar conditions and their current responses were studied in presence of 100 mg dl^{-1} cholesterol concentration. The biosensor shows excellent reproducibility as evident by low RSD of 1.85% for six different electrodes [Fig. 7B].

4. Conclusions

A one-step method for fabrication of functionalized nanostructured Au electrodes via electrochemical route has been demonstrated. The morphology and the hydrophilicity of the nanostructured Au electrode have been controlled using cysteamine. The variation of cysteamine concentration during fabrication enhances the electrochemical activity of the nanostructured Au electrode. The cysteamine molecules provide NH_2 terminations at the Au surface resulting in covalent functionalization of the bienzymes (ChEt-ChOx). The electrochemically deposited Au nanostructures onto the ITO substrates exhibit excellent electrocatalytic activity and enroute direct transfer of electrons from the immobilized enzyme molecules to the nanostructured electrode resulting in mediator-free 3rd-generation total cholesterol biosensor. The fabricated bioelectrode has been investigated for kinetic parameters and biosensing performance. The optimized bioelectrode exhibits high sensitivity of 0.53 A M^{-1} cm^{-2}, low detection limit of 1.57 μM and low K_m value of 0.63 mM due to facile and direct charge transportation across the interface. The proposed biosensor shows good selectivity, reproducibility and stability.

Acknowledgement

We thank Prof. R. C. Budhani (Director, NPL), Dr. A. M. Biradar and Prof. B. D. Malhotra for providing support and facilities, Dr. K. N. Sood for SEM measurements. R. S. is thankful to UGC-CSIR for award of Junior Research Fellowship. Financial support received from DST and CSIR Empower projects is sincerely acknowledged.

Supplementary Information

Scheme showing changes in the cyclic voltammograms after each modification step onto ITO, Cyclic voltammograms of the ChEt-ChOx/Glu-NanoAu/ITO bioelectrode in the presence of cholesterol and other interfering analytes.

References

1 T. K. Sau, A. L. Rogach, F. Jackel, T. A. Klar and J. Feldmann, *Adv. Mater.,* 2010**, 22**, 1805.
2 F. C. Chen, J. L. Wu, C. L. Lee, Y. Hong, C. H. Kuo and M. H. Huang, *Applied Physics Letters,* 2009**, 95**, 013305.
3 M. E. Stewart, C. R. Anderton, L. B. Thompson, J. Maria, S. K. Gray, J. A. Rogers and R. G. Nuzzo, *Chemical Reviews,* 2008**, 108**, 494.

4 B. D. Chithrani, A. A. Ghazani and W. C. W. Chan, *Nano Letters,* 2006**, 6**, 662.
5 P. K. Jain, K. S. Lee, I. H. El Sayed and M. A. El Sayed, *J. Phys. Chem. B,* 2006**, 110**, 7238.
6 M. Hu, J. Chen, Z. Y. Li, L. Au, G. V. Hartland, X. Li, M. Marquez and Y. Xia, *Chem. Soc. Rev.,* 2006**, 35**, 1084.
7 B. Duncan, C. Kim and V. M. Rotello, *J. Controlled Release,* 2010**, 148**, 122.
8 C. M. Cobley, J. Chen, E. C. Cho, L. V. Wang and Y. Xia, *Chem. Soc. Rev.,* **40**, 44.
9 P. Si, P. Kannan, L. Guo, H. Son and D. H. Kim, *Biosens. Bioelectron.,* 2011**, 26**, 3845.
10 M. C. Daniel and D. Astruc, *Chemical Reviews,* 2003**, 104**, 293.
11 L. Shi, Z. Chu, Y. Liu, W. Jin and X. Chen, *Biosens. Bioelectron.,* 2013**, 49**, 184.
12 H. Liu, Y. Tian and P. Xia, *Langmuir,* 2008**, 24**, 6359.
13 I. Zhitomirsky, *Journal of Materials Science,* 2006**, 41**, 8186.
14 C. J. Huang, P. H. Chiu, Y. H. Wang, K. L. Chen, J. J. Linn and C. F. Yang, *J. Electrochem. Soc.,* 2006**, 153**, D193.
15 L. Wang, X. Chen, X. Wang, X. Han, S. Liu and C. Zhao, *Biosens. Bioelectron.,* 2011**, 30**, 151.
16 R. Sharma, M. A. Ali, N. R. Selvi, V. N. Singh, R. K. Sinha and V. V. Agrawal, *J. Phys. Chem. C,* 2014**, 118**, 6261.
17 Z. Luo, K. Zheng and J. Xie, *Chem. Comm.,* **50**, 5143.
18 H. G. Liao, L. Cui, S. Whitelam and H. Zheng, *Science,* 2012**, 336**, 1011.
19 A. F. Azevedo, J. T. Matsushima, F. C. Vicentin, M. R. Baldan and N. G. Ferreira, *Appl. Surf. Sci.,* 2009**, 255**, 6565.
20 R. K. Dukor, J. M. Chalmers and P. R. Griffiths, *Vibrational Spectroscopy in the Detection of Cancer, John Wiley and Sons, New York,* 2001, 3335.
21 U. Koelle and A. Laguna, *Inorg. Chim. Acta,* 1999**, 290**, 44.
22 P. Lessner, J. Winnick, F. R. McLarnon and E. J. Cairns, *J. Electrochem. Soc.,* 1986**, 133**, 2517.
23 E. Laviron, *J. Electroanal. Chem. Inter. Electrochem.,* 1979**, 100**, 263.
24 E. Laviron, *J. Electroanal. Chem. Inter. Electrochem.,* 1979**, 101**, 19.
25 S. Bhattacharyya, M. T. Stankovich, D. G. Truhlar and J. Gao, *J. Phys. Chem. A,* 2007**, 111**, 5729.
26 M. Yamashita, M. Toyama, H. Ono, I. Fujii, N. Hirayama and Y. Murooka, *Protein Eng.,* 1998**, 11**, 1075.
27 A. Ahmadalinezhad and A. Chen, *Biosens. Bioelectron.,* **26**, 4508.
28 L. Zhu, L. Xu, L. Tan, H. Tan, S. Yang and S. Yao, *Talanta,* 2012**, 106**, 192.
29 Z. Matharu, P. Pandey, M. K. Pandey, V. Gupta and B. D. Malhotra, *Electroanalysis,* 2009**, 21**, 1587.
30 Z. Matharu, P. R. Solanki, V. Gupta and B. D. Malhotra, *Analyst,* 2012**, 137**, 747.

Tables

Table 1. Table showing the values of kinetic parameters for various nanostructured Au electrodes and the bioelectrode.

Electrodes	Cysteamine Conc. (mM)	Electron Transfer Coefficient, α	Charge Transfer Rate Constant, k_s (s^{-1})	Surface Conc., Γ (mol cm^{-2})
NanoAu/ITO	0	0.50	68.39	1.30×10^{-13}
NanoAu/ITO	0.025	0.56	18.90	1.32×10^{-13}
NanoAu/ITO	0.125	0.62	9.78	3.72×10^{-13}
NanoAu/ITO	0.625	0.65	3.55	8.22×10^{-13}
ChEt-ChOx/Glu-NanoAu/ITO	0.625	0.68	7.09	8.82×10^{-12}

Table 2. Comparison table summarizing the biosensing characteristics of the mediator-free cholesterol biosensors.

Matrix	Analyte	Sensitivity	Detection Limit	Linear Range	K_m^{app}	Ref.
ChOx/AuNPs-MWCNT/GCE	Free Cholesterol	-	4.3 µM	0.01-5 mM	0.29 mM	[28]
ChOx/Au-ODA/ITO	Free Cholesterol	1.08×10^{-3} $mAmM^{-1}$	0.60 mM	0.65-12.95 mM	0.5 mM	[29]
ChOx/4-ATP/Au	Free Cholesterol	542.3 $nAmM^{-1}$	-	0.62-10 mM	1.34 mM	[30]
ChOx-Glu/Cys-Au/ITO	Free Cholesterol	4.22 $mAmM^{-1}cm^{-2}$	5.41 µM	0.26-12.95 mM	0.57 mM	[16]
ChEt-ChOx/4-ATP/Au	Total Cholesterol	886.6 $nAmM^{-1}$	-	0.62-10 mM	1.06 mM	[30]
ChEt-ChOx/Glu-NanoAu/ITO	Total Cholesterol	0.53 $mAmM^{-1}cm^{-2}$	1.57µM	0.26-12.95 mM	0.63 mM	Present Work

Figures Caption

Scheme 1. Schematic illustration for the electrochemical synthesis of Au nanostructures, fabrication of the bienzymatic electrode and the detection scheme for the cholesterol ester.

Fig. 1. AFM images of Au films electrochemically deposited using $HAuCl_4$ with cysteamine concentration of (a) 0 mM, (b) 0.025 mM, (c) 0.125 mM and (d) 0.625 mM.

Fig. 2. (A) Contact angle of water drop with Au films deposited with cysteamine concentration of (a) 0 mM, (b) 0.025 mM, (c) 0.125 mM and (d) 0.625 mM. (B) FTIR spectra of (i) NanoAu/ITO, (ii) Glu-NanoAu/ITO and (iii) ChEt-ChOx/Glu-NanoAu/ITO.

Fig. 3. SEM images of (a) NanoAu/ITO, (b) Glu-NanoAu/ITO and (c) ChEt-ChOx/Glu-NanoAu/ITO.

Fig. 4. (A) Chronoamperometric response as a function of time during electrochemical deposition of Au nanostructures. (B) Cyclic voltammograms of nanostructured Au electrodes in phosphate buffer saline (pH 7.4) without mediator at scan rate of 50 mV s^{-1}. (C) Cyclic voltammograms as a function of scan rate for NanoAu/ITO electrode and (D) ChEt-ChOx/Glu-NanoAu/ITO bioelectrode in phosphate buffer saline (pH 7.4). Inset (i) Anodic and cathodic potential as a function of logarithmic value of scan rate. Inset (ii) Anodic and cathodic current as a function of square root of the scan rate.

Fig. 5. (A) Cyclic voltammograms of ITO electrode, NanoAu/ITO electrode, Glu-NanoAu/ITO electrode and ChEt-ChOx/Glu-NanoAu/ITO bioelectrode in phosphate buffer saline at scan rate of 50 mV s^{-1}. (B) Cyclic voltammograms of ChEt-ChOx/Glu-NanoAu/ITO bioelectrode in presence of cholesterol concentrations (10-500 mg dl^{-1}) in phosphate buffer saline (pH 7.4). (C) Calibration plot showing variation of anodic current with cholesterol concentrations. (D) Interference curve showing variation of anodic current as a function of different analytes.

Fig. 6. (A) Cyclic voltammetric response of the ChEt-ChOx/Glu-NanoAu/ITO bioelectrode for available clinical samples of different concentrations. (B) Calibration plot showing the variation of anodic peak current with cholesterol concentrations.

Fig. 7. (A) Shelf-life curve showing current response of the bioelectrode towards 100 mg dl^{-1} cholesterol concentration as a function of time. (B) Reproducibility curve showing current response of six bioelectrodes (prepared under similar conditions) towards 100 mg dl^{-1} cholesterol concentration.

Figures

Scheme 1

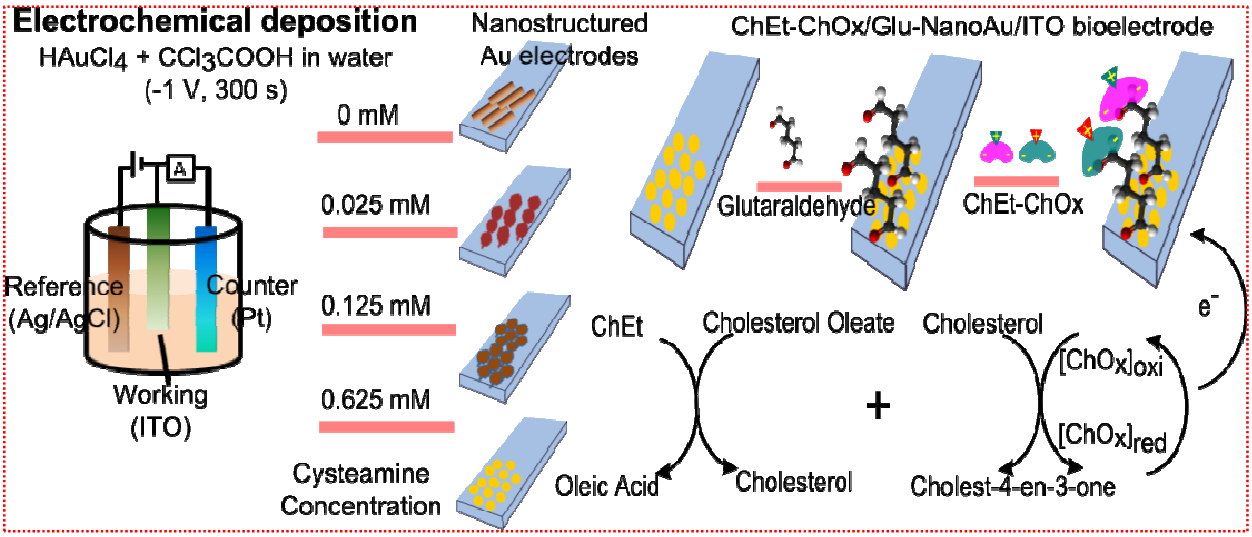

Figure 1

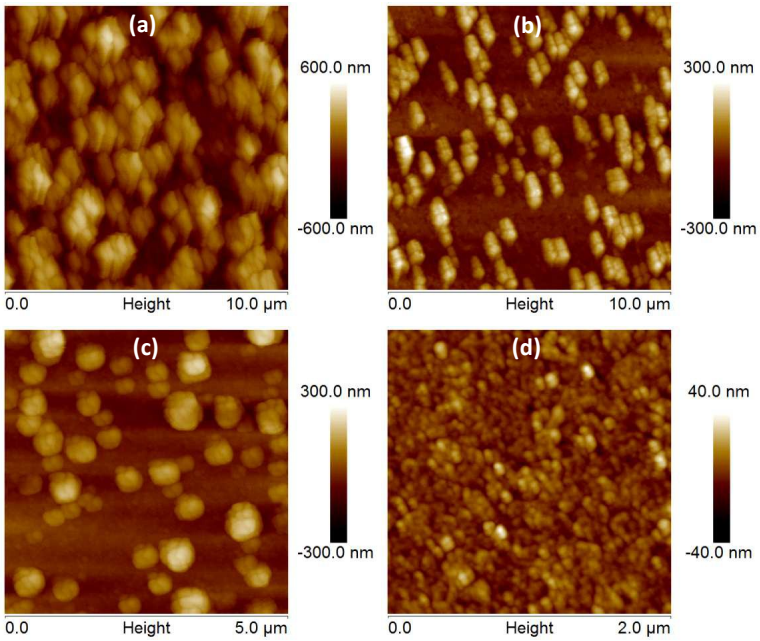

Figure 2

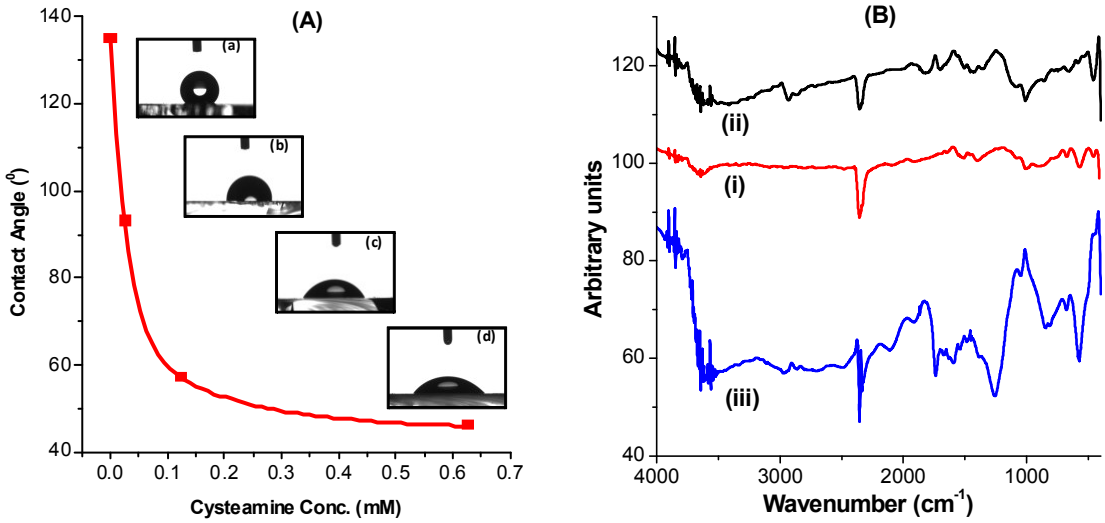

Figure 3

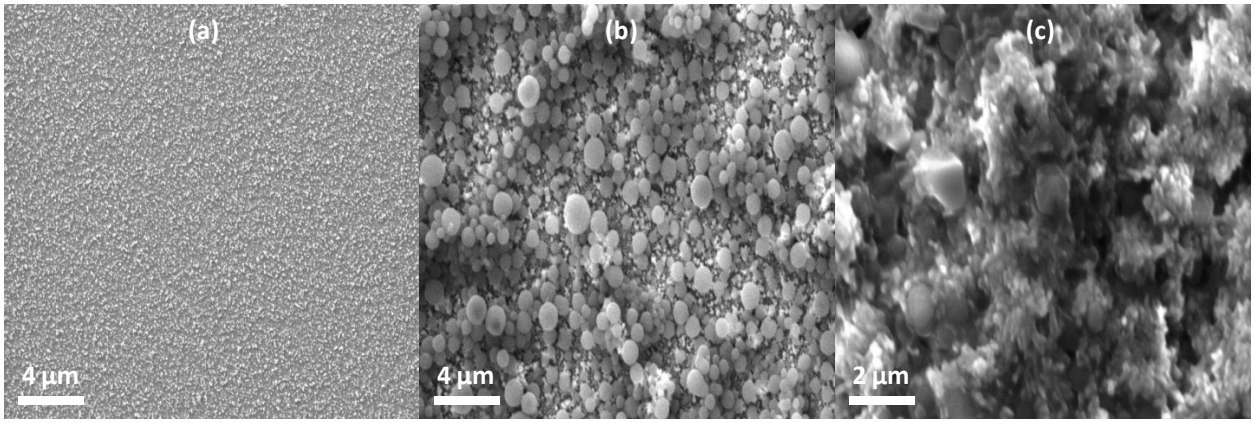

Figure 4

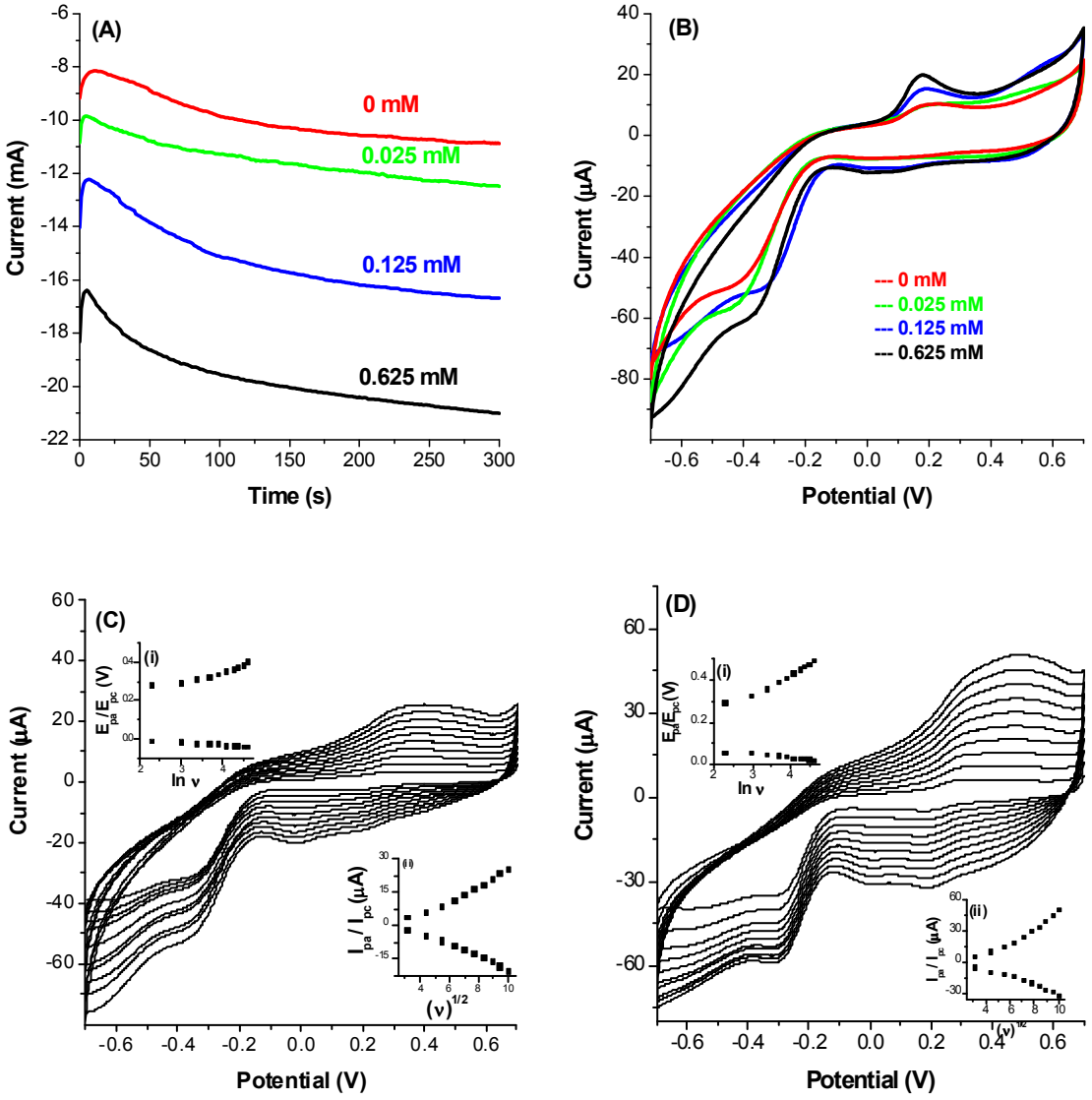

Figure 5

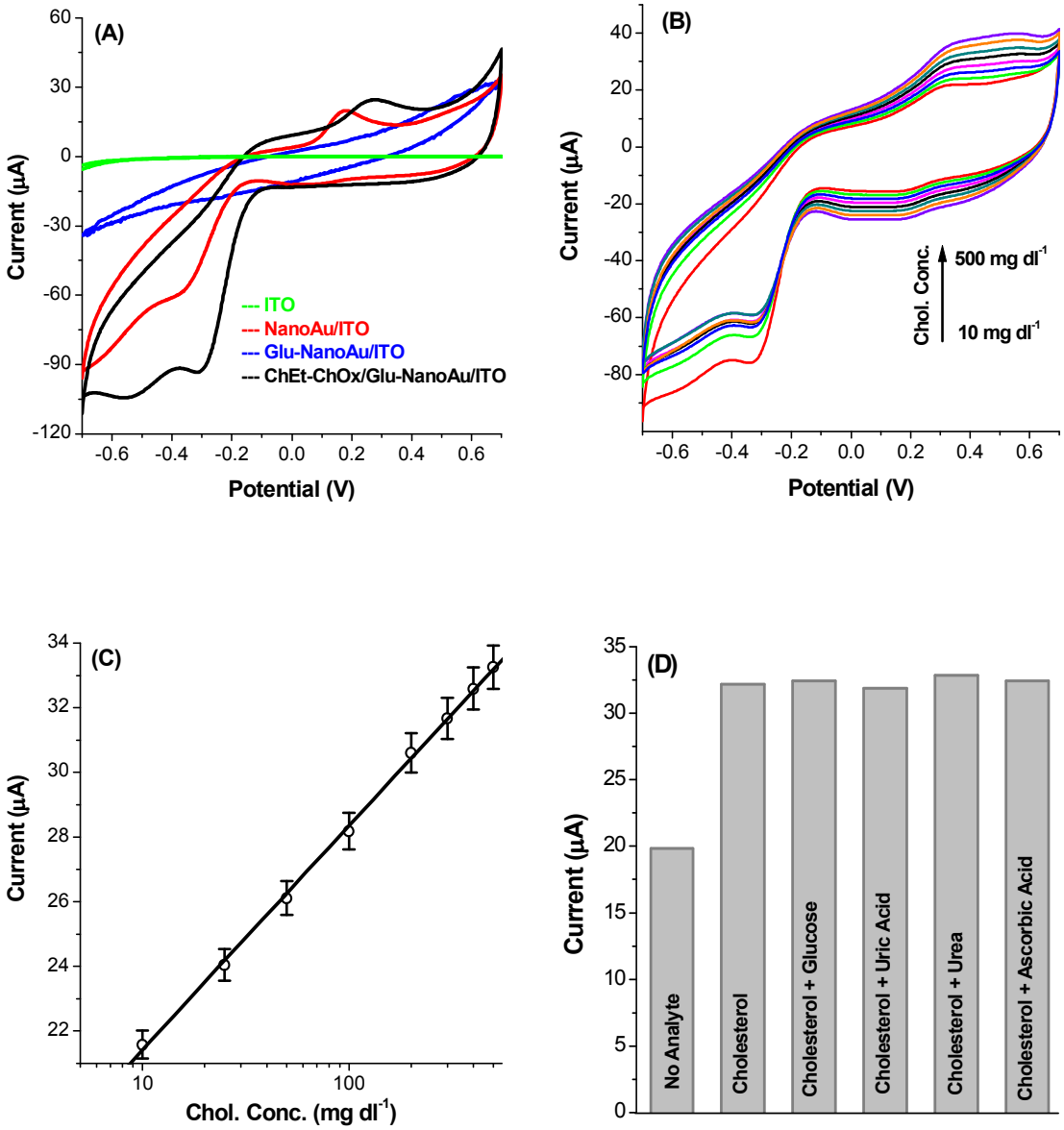

Figure 6

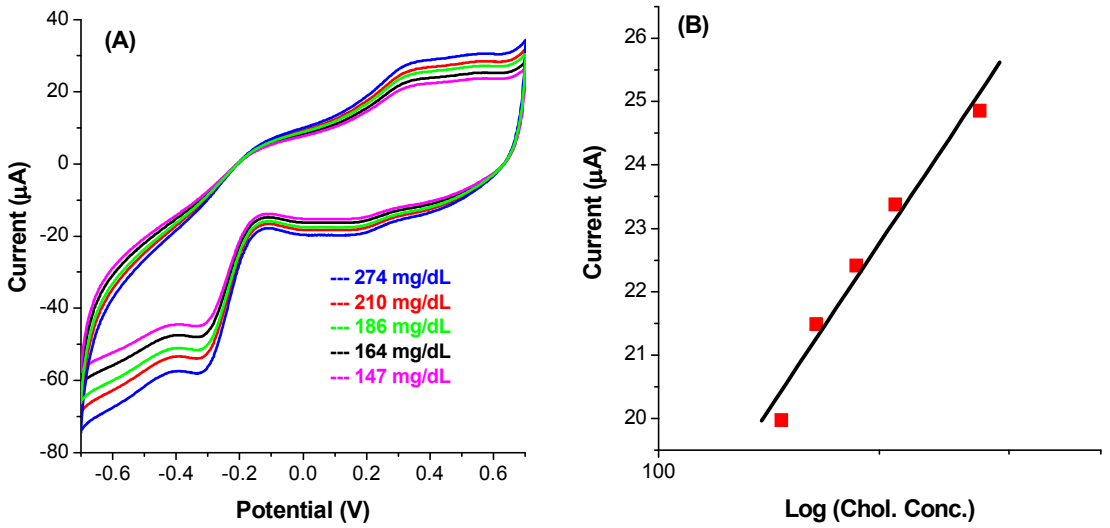

Figure 7

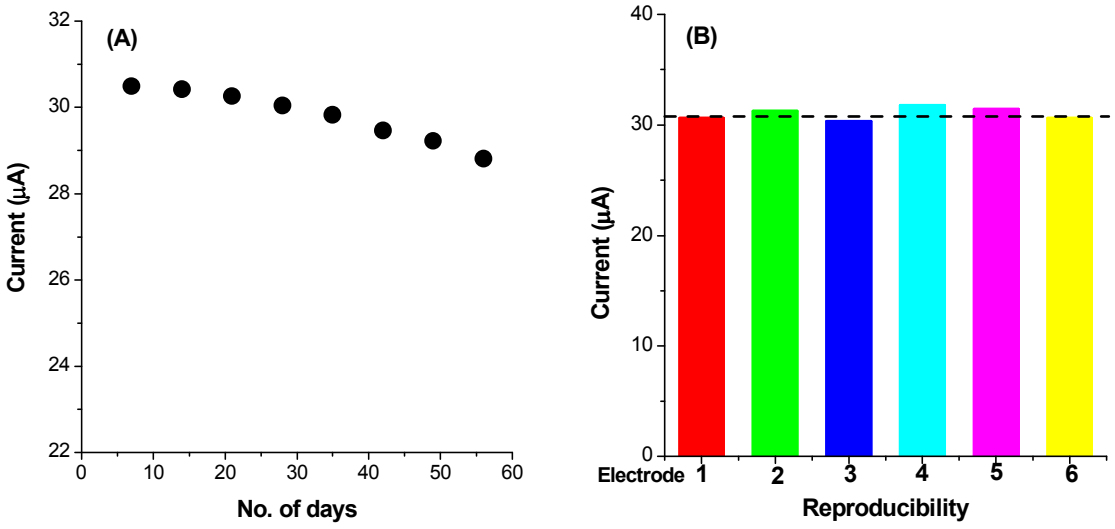

Table of Contents Entry

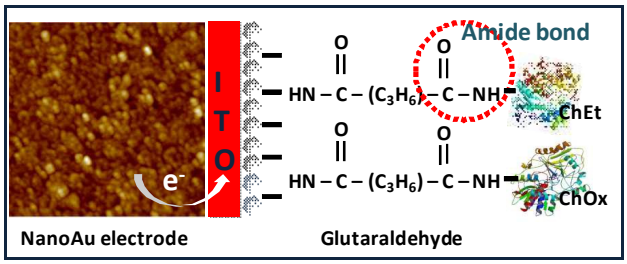

Novelty Statement

One-step electrochemical route for synthesis, functionalization and deposition of Au nanostructures and the bi-enzyme functionalization of Au electrode has been proposed.